Towards photo-CIDNP MAS NMR as a generally applicable enhancement method

Thamarath Surendran, S.

Chapter 2

Whole-cell NMR characterization of two photochemically active states of the photosynthetic reaction center in heliobacteria

---

2.1 *Abstract*

The photo-CIDNP (photochemically induced dynamic nuclear polarization) MAS (magic-angle spinning) NMR studies of light-induced spin-correlated radical pairs in whole cells of *Heliobacillus mobilis* demonstrate that heliobacterial reaction centers (RCs) are operational in two different states. A culture maintained anaerobically is called Braunstoff (German for brown substance). After exposure to oxygen, Braunstoff is converted to Grünstoff (green substance) as indicated by a color change due to the conversion of BChl *g* to Chl *a*. It is shown that electron transfer occurs symmetrically via both branches of cofactors in both forms. The donor and acceptor cofactors remain identical and unchanged upon conversion while the intermediate accessory cofactors are transformed from BChl *g* to Chl a_F. The donor triplet state in Braunstoff is localized on the special pair donor and lives for 100 μs, demonstrating the presence of a long lived donor triplet state which is not quenched, *e.g.*, by nearby carotenoids. In Grünstoff, the donor triplet becomes mobile and appears to be formed on an accessory cofactor.

This chapter is published in *Biochemistry* 51, 5763-5773 (2012).

2.2 *Introduction*

Heliobacillus (Hb.) mobilis is a strictly anaerobic, nitrogen fixing photosynthetic organism found in abundance in rice paddy fields.[1-3] The photosynthetic machinery of *Hb. mobilis* contains antenna pigments and most of the RC cofactors are bound to a single polypeptide dimer in the cytoplasmic membrane. *Hb. mobilis* has a Type I RC similar to PSI in having an iron-sulfur cluster F_X as a bound electron acceptor.[4] Because it is a homodimer and has a simple polypeptide composition, the heliobacterial RC has been proposed as the evolutionary ancestor of PSI.[5,6] The more complex heterodimeric PSI may thus have evolved by a simple gene duplication event.[7] Unlike other photosynthetic bacteria, *Hb. mobilis* contains few complex structures such as intercytoplasmic membranes and it has no chlorosomes.[1,8] Due to its less complex structure, the heliobacterial RCs would represent attractive models for understanding the homodimeric RCs.[3] However, thus far there is very little structural information available for the heliobacterial RC.

The absorption spectrum of anaerobic *Hb. mobilis* cells is shown in Figure 2.1 (solid line). The color appears brownish green and it is therefore called here Braunstoff. A unique pigment, bacteriochlorophyll *g* (BChl *g*, see Figure 2.2 A), has been identified in these bacteria.[9] BChl *g* acts as antenna pigment and two 13^2 epimers (BChl *g*') act as the primary electron donor special pair ($P798^+$).[10] The primary electron acceptor is 8^1-hydroxy chlorophyll a_F (8^1-OH Chl a_F, Figure. 2.2 B).[11,] The intense absorbance peaks at 570 nm and 798 nm correspond to BChl *g*. The less intense peak at 670 nm corresponds to 8^1-OH Chl a_F.[11,12] Both isolated RCs and membranes have been studied by FT-IR,[13] EPR techniques,[14] and photo-CIDNP MAS NMR[15].

A peculiarity of BChl *g* is the photoconversion at pyrrole ring II when exposed to oxygen in the presence of light. The color change from brownish green to emerald green is observed during this process[3] and leads to a product called Grünstoff here. The pigment becomes spectroscopically equivalent to Chl a_F, which is present in cyanobacteria and green plants.[3] The absorption spectrum of *Hb.*

mobilis after this process is shown in Figure 2.1 (dotted line). All absorbance peaks of BChl *g* pigments decrease upon the conversion. The small remaining peak at 798 nm indicates that the conversion is almost complete. The peak at 670 nm, indicating Chl a_F, becomes more intense. There is not much information available

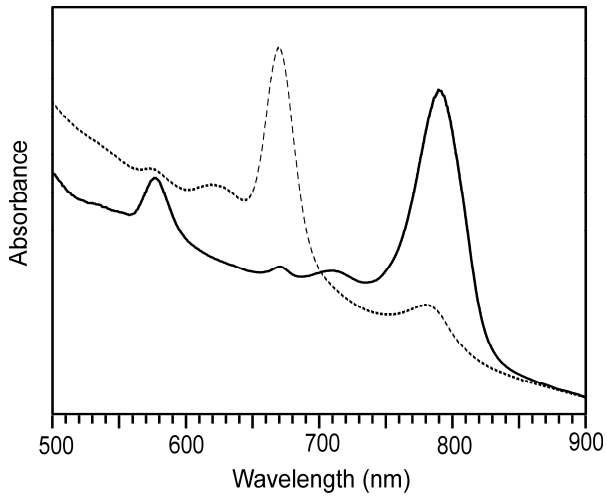

Figure 2.1: Absorption spectra of heliobacterial cells in the anaerobic (Braunstoff, solid line) and aerobic (Grünstoff, dashed line) states. The absorbance is presented in arbitrary units.

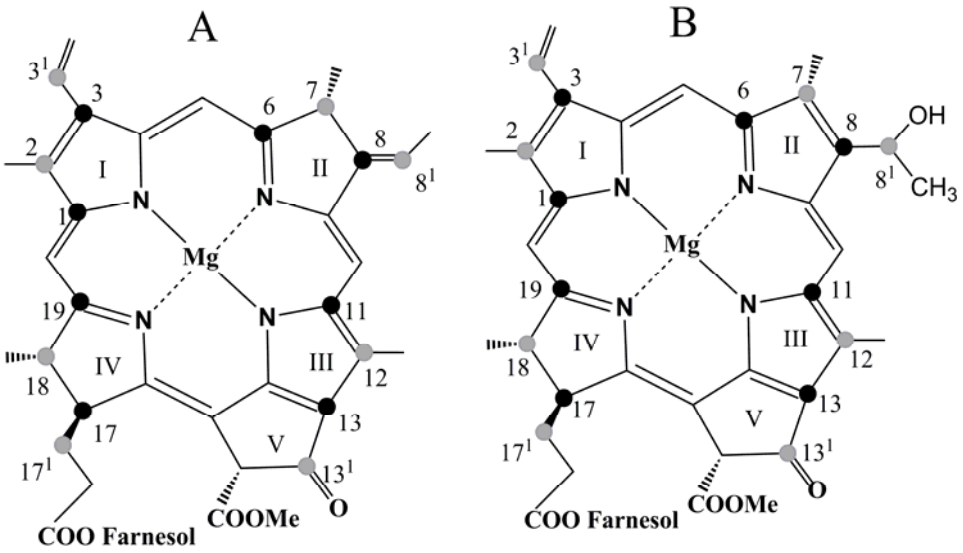

Figure 2.2: BChl *g* (A) and 8^1-OH BChl a_F (B) with label patterns obtained by feeding 4-ALA (black) or 3-ALA (gray). The double bond and metal coordination pattern represents the predominant resonance structure for the bacteriochlorin (A) and the chlorin (B), and follows the corresponding pheophorbides, with >N- pyrrole type nitrogens in rings I and III, and ≥N| pyridine type nitrogens in rings II and IV.

about Grünstoff other than its absorption spectrum.[3] The present work demonstrates that in heliobacterial RCs under aerobic conditions, radical pairs are also formed in Grünstoff by light-induced electron transfer. Here, both Braunstoff and Grünstoff are studied by ^{13}C and ^{15}N photo-CIDNP MAS NMR directly at the cellular level.

The solid-state photo-CIDNP effect, discovered in 1994 by Zysmilich and McDermott[16] has been observed in all natural RCs studied and the effect may well be an intrinsic property of light-induced electron transfer in photosynthesis.[17] In this effect, non-Boltzmann nuclear spin polarization is detected as strongly enhanced ^{13}C or ^{15}N MAS NMR signals.[18] Nuclear spin polarization is established

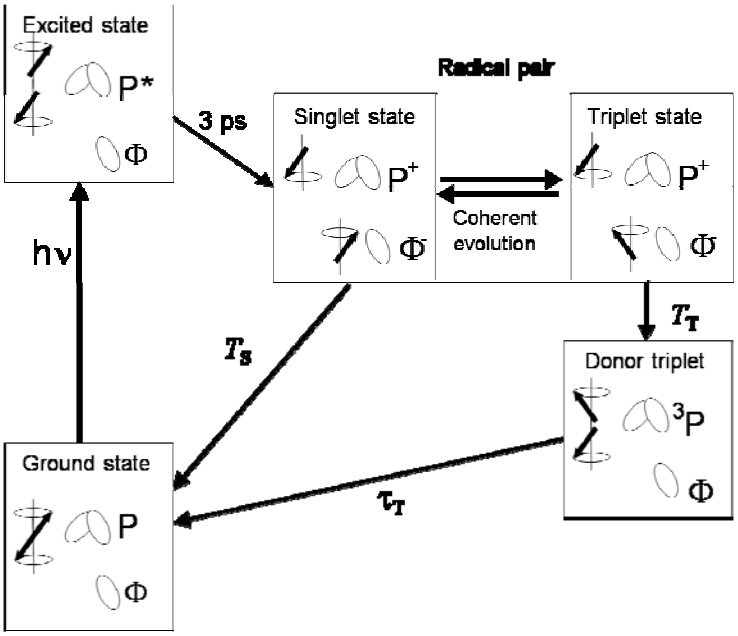

Scheme 2.1: Photocycle in quinone-depleted RCs of *Rb. sphaeroides* WT and R26. Upon illumination and fast electron transfer from an excited singlet state, a radical pair is formed in a pure singlet state having high electron spin order. The radical pair is formed by a radical cation at the two donor BChls (Special pair, P) and a radical anion on the BPhe acceptor cofactor (Φ) of the active branch. The chemical fate of the radical pair depends on its electronic spin state: the singlet state is allowed to recombine with the lifetime of T_S = 20 ns and this recombination pathway is termed singlet channel. For the triplet state a direct recombination is spin-forbidden and a donor triplet (^3P) is formed with a lifetime of T_T= 1 ns. The lifetime of the donor triplet state (τ_T) is 100 ns for WT RCs and 100 μs for R26 RCs. The recombination pathway of the donor triplet to the ground state is termed triplet channel. Mechanisms building up photo-CIDNP under steady-state conditions are TSM, DD and DR. Transient nuclear polarization is observed in time-resolved experiments and includes a contribution from the RPM.

by symmetry breaking of the correlated radical pair state via the hyperfine interaction.[19] At the high magnetic fields as applied in an NMR experiment, it is explained by one or more of three parallel mechanisms that can occur in the solid state with continuous illumination:[20-22] three spin mixing (TSM),[23] differential decay (DD)[24] and differential relaxation (DR).[25]

These mechanisms are well understood in photo-CIDNP MAS NMR studies of the quinone-depleted RCs of *Rb. sphaeroides* and in theoretical simulations based on these experiments.[19,22] Scheme 2.1 shows the spin chemical cycle processes that lead to strong nuclear polarization in RCs of *Rb. sphaeroides* WT and its carotenoid less mutant R26. By illumination with white light, the primary electron donor, which is a special pair of BChl *a* molecules, is excited and forms a radical cation by donating an electron to the primary electron acceptor Φ, BPhe *a*. This leads to the formation of a spin-correlated radical pair, initially in its singlet state (S), which is not an eigenstate and converts to the triplet state (T_0) and back by coherent evolution. The high electron spin order of the initial pure electronic singlet state is transferred to a net nuclear polarization by two parallel and competing mechanisms termed TSM[23] and DD.[24] The TSM mechanism is explained by the combined action of electron-electron dipolar coupling or exchange coupling and the pseudosecular hyperfine coupling (hfc) $B = (A_{zx}^2 + A_{zy}^2)^{1/2}$, which breaks the antisymmetry of $\langle I_z \rangle$ nuclear spin population in coherent spin evolution of the spin correlated radical pair.[23] Due to different lifetimes of the S and of the T_0 states, antisymmetry of the nuclear spin population in the spin correlated radical pair can be broken by a buildup of net nuclear polarization via the *B* in a DD mechanism. The polarization transfer by the DD mechanism occurs due to a single matching condition of $2|\omega_I| = |A_{zz}|$, and the difference of singlet and triplet radical pair lifetimes must be of the order of the inverse hyperfine splitting, *i.e.* $|T_T^{-1} - T_s^{-1}| \sim [(\omega_I + A/2)^2 + B^2/4)]^{1/2} - [(\omega_I - A/2)^2 + B^2/4)]^{1/2}$. The electron Zeeman interaction drives nuclear-spin independent interconversion between the singlet and triplet state of the radical pair, thus not affecting nuclear spin populations. This remains true even in the presence of *B*, since this coupling is too small to mix different electron spin states. Only if electron spin states are mixed by electron-electron coupling (*d*), as in the TSM mechanism, mixing of nuclear spin states by *B* will also be affected by an

electron spin state mixing. If the singlet and triplet state of the radical pair have different lifetimes, as in the DD mechanism, pairs in these two states will experience hyperfine evolution for a different time, which also breaks the antisymmetry of the nuclear spin populations. For B=0 the contribution of the nuclear Zeeman interaction (ω_I) to spin evolution is independent of the electron spin state and will thus not lead to any polarization transfer. For $B\neq0$ the ratio $|\omega_I/A_{zz}|$ determines the extent of mixing of the nuclear spin states, and thus also the extent to which population antisymmetry is violated. Maximum mixing occurs if the ratio is one. The emissive signals of the photo-CIDNP MAS NMR spectrum of WT RCs are due to the predominance of the TSM mechanism over the DD mechanism, and the contribution of the DD to emissive/absorptive patterns depends on the Δg for the two electron spins involved, which is negative for BChl and BPheo.[19] The relative intensity of these emissive photo-CIDNP MAS NMR signals provides information about the spin density distribution of the radical pair in RCs.[20] In the carotenoid-less mutant R26 of *Rb. sphaeroides,* RCs that have a long lived donor triplet, polarization transfer by a DR mechanism occurs in addition.[21,25] This is a modified RPM and depends on the different nuclear longitudinal relaxation rates.[19,26,27]

While electron polarization does not build up during subsequent photocycles, the long ^{13}C longitudinal nuclear relaxation time (T_1)[18] allows for the accumulation of nuclear polarization in a photo-CIDNP MAS NMR experiment. During subsequent photocycles, the electron spin order is transferred to nuclear polarization and during the ^{13}C T_1 time, this nuclear polarization can be accumulated in a steady-state photo-CIDNP experiment since the ^{13}C T_1 is longer than the time constant for nuclear polarization build up. The CIDNP effect can be invoked without quinone depletion by providing high light that reduces the secondary acceptor and blocks the transfer of electrons along the photosynthetic conversion chain. It has been shown to allow for a signal enhancement of more than 10000 relative to the signal in the dark, and hence for the detection of cofactors directly in whole cells.[21,28] Recently, it has been demonstrated that the effect is not limited to frozen natural photosynthetic RCs at NMR fields, but it also occurs in a blue-light photoreceptor (see chapter 4), in liquid membranes,[29] and is

predicted to occur at earth's field.[30] Since the effect relies on hyperfine interactions, it requires a radical pair lifetime of at least some tens of nanoseconds. Hence, any observation of the effect implies that light-induced radical pairs with a lifetime significantly longer than ten nanoseconds are generated in a sample.

In time-resolved experiments, the RPM, TSM, DD and DR mechanisms can lead to transient nuclear polarization.[31] In particular for R26 samples, the electronic ground state can be formed from the radical pair in its singlet state on a time scale T_s = 20 ns, while for the triplet state of the radical pair the decay to the ground state takes much longer, τ = 100 μs (Scheme 2.1). Since the nuclear hyperpolarization on this triplet pathway is partially extinguished by longitudinal relaxation, the nuclear polarization from the singlet pathway is observed selectively. This enables the observation of transient nuclear polarization selectively from the singlet state during the lifetime of the donor triplet.[22]

The work in this chapter builds upon and extends the initial studies of Roy *et al.* on the photo-CIDNP effect in heliobacteria (Braunstoff) on the membrane level.[15] Due to the presence of a long-lived donor triplet, a strong contribution of DR mechanism to the photo-CIDNP effect in Braunstoff was observed. In this chapter, the previous work is extended to a detailed analysis of Braunstoff at the cellular level and the photoconversion of heliobacterial cells to Grünstoff is described. In addition, a detailed study of both forms of heliobacteria using different isotope label incorporation and by time-resolved photo-CIDNP MAS NMR experiments is performed. This resolves the contribution of different mechanisms for the photo-CIDNP effect in both Braunstoff and Grünstoff and provides a concept about the functional mechanisms and the changes in the RC induced by the photoconversion.

2.3 *Materials and Methods*

2.3.1 *Sample Preparation*

Cells of *Hb. mobilis* strain ATCC 43427 (DSMZ 6151) were used in this study. The cells were cultured in medium no. 1552[32] anaerobically at 37ºC with continuous light. After seven days of growth, cells were harvested by centrifugation (4000 rpm). One half of the harvested cells were uniformly

suspended in deoxygenated 20 mM Tris HCl buffer (pH = 8) containing 10 mM sodium ascorbate. In a dry nitrogen gas flow, the Braunstoff sample was reduced with 50 mM sodium dithionite and packed in a 4-mm sapphire rotor for MAS NMR experiments. The other half of the harvested cells was used for preparing Grünstoff. These cells were washed with the medium no.1552 that does not contain sodium ascorbate. The cells were resuspended in the same non-ascorbate medium and were bubbled with oxygen gas under illumination. The conversion to Grünstoff was monitored by taking absorption spectra every 15 minutes. After 3 hours, the conversion to Grünstoff was almost complete and the cells were collected by centrifugation. The cells were resuspended in 20 mM Tris HCl buffer (pH = 8) containing 10 mM sodium ascorbate and reduced with 50 mM sodium dithionite under a nitrogen gas flow. The Grünstoff sample was packed in a 4 mm sapphire rotor for the MAS NMR experiments.

Since NH_4^+ ions appear to be the nitrogen source for the chlorophylls in *Hb. mobilis* cells,[8] $^{15}NH_4Cl$ was used as the precursor for ^{15}N labeling. The *Hb. mobilis* cells were grown anaerobically in medium no. 1552, which contained 46 mM $^{15}NH_4Cl$. The conversion to Grünstoff and the preparation of Braunstoff and Grünstoff samples for ^{15}N MAS NMR experiments was carried out as described above. For selective ^{13}C isotope labeling of BChls and Chls,[33] *Hb. mobilis* cells were grown anaerobically in medium no.1552 containing 1 mM [4-^{13}C]-δ-aminolevulinic acid (ALA) or 3-^{13}C ALA. The carbon atoms C-1, C-3, C-6, C-8, C-11, C-13, C-17 and C-19 of the two BChl species (Figure 2.2, black labels) are selectively isotope labeled by 4-^{13}C ALA incorporation. The 3-^{13}C ALA incorporation produces selective ^{13}C isotope labeling of C-2, C-3^1, C-7, C-8^1, C-12, C-13^1, C-17^1, C-18 carbon atoms of the BChls (Figure 2.2, gray labels). The conversion of Braunstoff to Grünstoff was carried out for both 4-^{13}C ALA and 3-^{13}C-ALA labeled *Hb. mobilis* cells as described above. The 4- and 3-^{13}C ALA labeled Braunstoff and Grünstoff samples were reduced by 50 mM sodium dithionite and packed in 4 mm sapphire rotors for ^{13}C MAS NMR measurements.

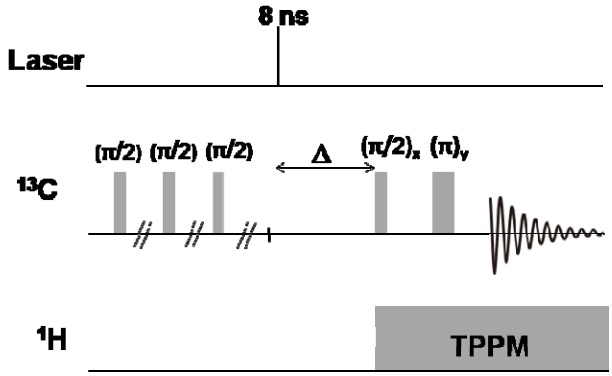

Figure 2.3: Pulse program for time-resolved photo-CIDNP MAS NMR experiments. The delay time Δ is the time difference between the nanosecond laser pulse and the NMR pulse.

2.3.2 *MAS-NMR Measurements*

^{13}C and ^{15}N MAS NMR experiments of *Hb. mobilis* cells were measured with a DMX-200 MHz spectrometer equipped with a 4-mm MAS probe (Bruker, Karlsruhe, Germany). The sample was packed into an optically transparent 4-mm MAS sapphire rotor and inserted into the MAS probe. A very low spinning frequency of 500 Hz was applied during freezing to achieve a homogeneous distribution of sample against the rotor wall.[34] The spinning frequency was increased to 8 kHz after the sample was completely frozen at 235 K.

For continuous illumination photo-CIDNP MAS NMR experiments, white light from a 1000 W xenon lamp was used. Both dark and photo-CIDNP spectra were obtained with a simple Hahn echo pulse sequence[35,36] with TPPM proton decoupling.[37] Laser flashes with pulse lengths of 6-8 ns and energy of 20 mJ were used for time resolved photo-CIDNP MAS experiments. The 532 nm laser flashes were produced using a Nd:YAG laser (SpectraPhysics Quanta-Ray INDI 40-10, Irvine CA, USA). The Hahn echo pulse sequence with TPPM proton decoupling was used for the time resolved photo-CIDNP MAS NMR experiments (Figure 2.3). Additional ^{13}C presaturation pulses were also used prior to a new scan to scramble the remaining ^{13}C coherence and polarization.[31] The nanosecond laser flash was synchronized with the $\pi/2$ pulse at the start of the Hahn-echo pulse sequence using an external 500 MHz oscilloscope. The delay time Δ is the time difference between the nano-second laser flash and the $\pi/2$ NMR pulse.

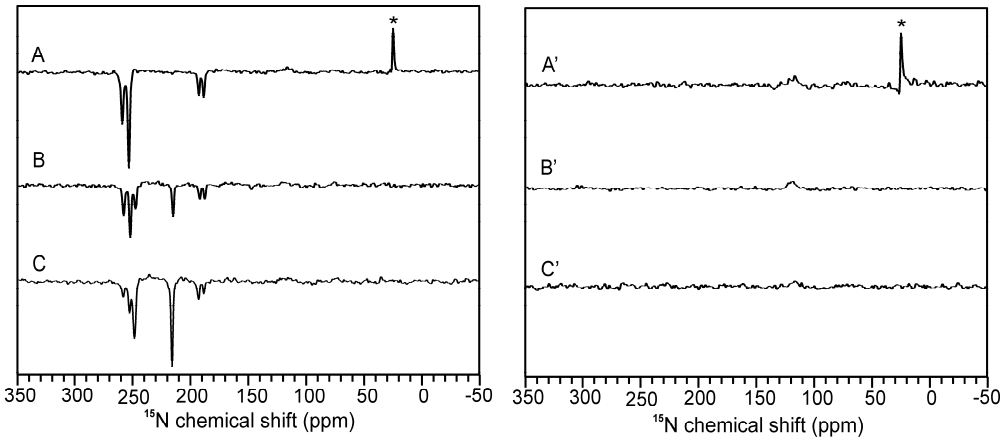

Figure 2.4: ^{15}N MAS NMR spectra of anaerobically (Braunstoff) (A, A'), half-converted (anaerobic/aerobic) (B, B'), aerobically treated (Grünstoff) (C, C') uniformly ^{15}N labeled cells of *Hb. mobilis* cells obtained by illumination with continuous white light (left side) and the data collected in the dark (right side). The spectra have been obtained in a magnetic field of 4.7 T and at a temperature of 235 K. The asterisk on the signal at 23 ppm indicates remaining $^{15}NH_4^+$ ions in the sample.

In the NMR experiments, a recycle delay of 2s was applied. ^{13}C MAS NMR signals of cells with ^{13}C in natural abundance and ^{13}C-ALA labeled *Hb. mobilis* cells were collected for 40 h, and 12 h respectively. ^{13}C time resolved experiments were carried out for 9 h in 3-^{13}C ALA labeled *Hb. mobilis* cells. Both dark and light ^{13}C MAS NMR spectra were referenced to the ^{13}COOH chemical shift of solid tyrosine•HCl at 172.1 ppm and artificial line broadening of 50 Hz was applied prior to Fourier transformation. All ^{15}N MAS NMR spectra were collected for 40 h. Chemical shifts are given relative to the $^{15}NH_3$ resonance frequency, using the response of solid $^{15}NH_4NO_3$ at δ = 23.5 ppm as a reference. For ^{15}N MAS NMR spectra, artificial line broadening of 20 Hz was applied prior to Fourier transformation. ^{13}C and ^{15}N photo-CIDNP MAS NMR spectra were normalized with the most intense signal in each spectrum.

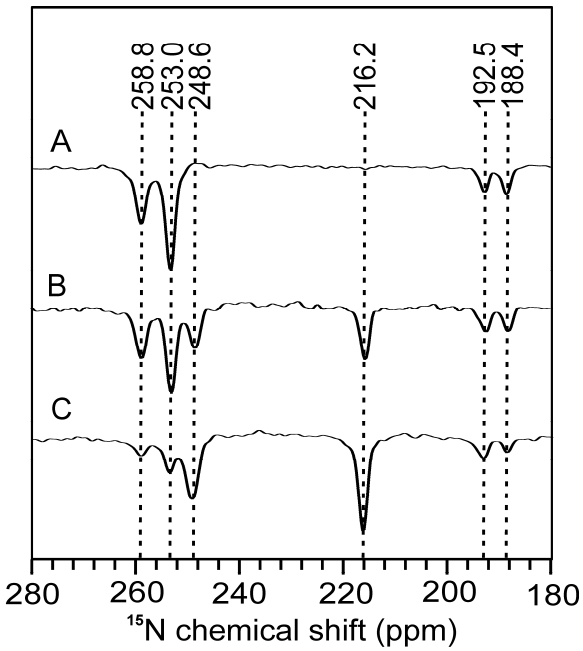

Figure 2.5: Expanded view of ^{15}N photo-CIDNP MAS NMR spectra of anaerobically (Braunstoff) (A), half-converted (anaerobic/aerobic) (B), aerobically treated (Grünstoff) (C) uniformly ^{15}N labeled cells of *Hb. mobilis* cells, obtained by illumination with continuous white light.

2.4 *Results*

2.4.1 *^{15}N photo-CIDNP MAS NMR experiments*

The present work demonstrates that the solid-state photo-CIDNP effect is observable by ^{15}N MAS NMR in whole cells of both forms of uniformly ^{15}N labeled *Hb. mobilis* (Figure 2.4 and Figure 2.5). Since the build-up of photo-CIDNP requires radical pair lifetimes of at least some tens of nanoseconds (Fig 2.1), the occurrence of the effect demonstrates that this condition is fulfilled in both forms, Braunstoff and Grünstoff. In addition to the spectra of the two forms of *Hb. mobilis* cells, the spectrum of a half-converted sample is also shown (Spectra B and B' in Figure 2.4). The respective ^{15}N MAS NMR spectra (A', B' and C') measured in the dark are shown in the right panel of Figure 2.4. In ^{15}N MAS spectra collected in the dark, only signals from the protein backbone are visible, while light induced signals appear in the ^{15}N photo-CIDNP MAS NMR spectra. These light-induced ^{15}N MAS NMR signals of *Hb. mobilis* cells show emissive signs reminiscent of ^{15}N labeled RCs of *Rb. sphaeroides* [16,40] and of PSII.[38] In Figure 2.4, both ^{15}N MAS

NMR spectra collected in the dark (A') and with light (A) show a narrow signal at 23.5 ppm due to the presence of free NH_4^+ ions. During conversion of *Hb. mobilis* cells to Grünstoff, the cells were resuspended in a medium that does not contain $^{15}NH_4Cl$. Therefore, the signal at 23.5 ppm is absent in spectra (B, B') and (C, C').

Figure 2.5 shows an expanded view of the ^{15}N photo-CIDNP MAS NMR spectra in Braunstoff (A) as well as of half converted (B) and in Grünstoff (C) *Hb. mobilis* cells. In spectrum A, four signals appear, with chemical shifts of 188.4, 192.5, 253.0 and 258.8 ppm. ^{15}N photo-CIDNP MAS NMR provides less complex data compared to ^{13}C, allowing for a more straightforward analysis.[38,39] A tentative assignment (Table 2.1) of these signals was performed by comparison to similar data collected from Chl *a* in PSI and PSII[38] and BChl *a* of *Rb. sphaeroides* R26.[16,39] In BChl *g*, pyrrole ring II is different from that of Chl *a* and similar to that of BChl *a*. The data confirm that all ^{15}N light-induced MAS NMR signals in the spectrum of Braunstoff are due to the four nitrogen atoms of BChl *g*' of the donor while the signals from the putative acceptor 8^1-OH Chl a_F are not observed[15]. For ^{15}N NMR data, the distinction between pyrrole and pyridine nitrogens is straightforward, as is the recognition of a chlorin-type response. However, a full assignment of N-I, N-II, N-III and N-IV is not straightforward, only the ^{15}N-II for the chlorin is clear. The ^{15}N chemical shifts at 188.4 ppm, 258.8 ppm, 192.5 ppm and 253.0 ppm are thus tentatively assigned to the N-I, N-II, N-III and N-IV nitrogen atoms of BChl *g*', respectively. The primary donor in *Hb. mobilis* RCs was proposed to be a homodimer of BChl *g*' molecules.[10] The heterodimeric donor of PSI show broadening and splitting of ^{15}N signals in its spectra,[38] and a pronounced splitting of photo-CIDNP signals was observed in the case of chemically identical cofactors of the special pair of *Rb. sphaeroides*[20]. Thus it is possible that two cofactors give rise to the same response by lack of both static and dynamic heterogeneity, or that dynamic heterogeneity leads to a single response of one of the two cofactors depending on the trajectory along collective vibrational modes of the two BChl *g*' comprising the homodimeric donor.[41]

In spectrum (B), in addition to four signals from BChl *g*', two signals with chemical shifts of 216.2 and 248.6 ppm appear and the intensities of the signals at 253.0 and 258.8 ppm decrease. The signals at 216.2 and 248.6 ppm can be

Assignment	Chl a^*		BChl a^+	BChl g	8^1-OH Chl *a*
Atom	PS-I σ_{solid}	PS-II σ_{solid}	σ_{solid}	σ_{solid}	σ_{solid}
N-I	186.2 (e)		187.2	188.4	188.4
	190.9 (a)		189.3		
N-II	206.1 (a)	211.5 (e)	261.2	258.8	216.2
	211.5 (e)		251.0		
N-III	193.2 (a)	195.3 (e)	197.4	192.5	192.5
			191.9		
N-IV	233.3 (a)	247.6 (e)	255.9	253.0	248.6
	250.3 (e)		258.8		
	254.9 (e)				

Table 2.1: Tentative assignments of ^{15}N photo-CIDNP MAS NMR signals. Chemical shifts are referenced to liquid ammonia with use of an external standard of solid $^{15}NH_4NO_3$ ($\delta = 23.5$).

*^{15}N-photo-CIDNP MAS NMR data collected from PSI and PSII, where the emissive signals (e) are from the donor and the absorptive signals (a) from the acceptor Chl (38).

+^{15}N-photo-CIDNP MAS NMR on R26 (39).

attributed to the N-II and N-IV nitrogen atoms of the primary electron acceptor 8^1-OH Chl a_F (Table 2.1). In spectrum (C), the signals at 216.2 and 248.6 ppm (N-II and N-IV of 8^1-OH Chl a_F) are stronger than the signals at 253 and 258.8 ppm (N-II and N-IV of BChl *g*'), which decrease further in intensity relative to the data in Figure 2.5B. The two ^{15}N NMR signals at 188.4 and 192.5 ppm (N-I and N-III) remain unchanged during the conversion, implying that the chemical shifts are similar in both BChl *g*' and 8^1-OH Chl a_F cofactors.

For the Braunstoff, a long donor triplet lifetime τ leads to a predominant contribution of the DR mechanism to the photo-CIDNP effect.[15] The DR mechanism operates mainly on donor cofactors, with very little contribution from the acceptor.[21] In contrast, for the data collected from the Grünstoff, the observation of acceptor signals in addition to the donor signals indicates changes of the electron-electron coupling upon photoconversion. Since emissive signals are

generally attributed to TSM (Fig 2.1), the acceptor signals can be explained by the increase of the contribution from the TSM mechanism relative to the DD contribution. The mixed sample (Spectrum B) does not show any additional signal that would not belong to Braunstoff or Grünstoff. This suggests that the transformation does not lead to metastable asymmetric intermediate states in which one half of the RC is transformed and the other not.

It appears that the chemical constitution of the donor remains unchanged. Hence the color change is not caused by a change in the donor cofactors. Since also the acceptor signals in Grünstoff are not split, it appears that the strongly symmetric character remains intact upon transformation.

Assuming that the photo-CIDNP intensities of steady-state experiments correlate with electron spin densities in *p*-orbitals,[38] a similarity to PSII is observed in Braunstoff , with the highest electron spin density on a pyridine-type nitrogen, probably the N-IV.[38] On the other hand, the highest electron spin density of Grünstoff is observed on the N-II nitrogen atoms, and this is similar to PSI.[38].

2.4.2 *^{13}C photo-CIDNP MAS NMR on natural abundance samples*

The next step is to demonstrate that the solid-state photo-CIDNP effect can be observed in both natural abundance (n.a.) Braunstoff and Grünstoff *Hb. mobilis* cells by ^{13}C MAS NMR. In spectra A and C of Figure 2.6, the samples are measured in the dark and only weak and broad features from the protein are visible. Spectra B and D are the ^{13}C photo-CIDNP spectra of Braunstoff and Grünstoff, respectively, obtained with continuous illumination. Several light induced signals are observed in the region between 200 and 80 ppm. The ^{13}C photo-CIDNP spectrum of Braunstoff shows emissive (negative) and absorptive (positive) light-induced signals, comparable to those of RCs from *Rb. sphaeroides* R26[21] and PSII.[42] The long-lived donor triplet state (^{3}P) favors a strong contribution from the DR mechanism to the photo-CIDNP effect, which matches the ^{15}N data in Fig 2.5 and validates the early photo-CIDNP studies that were performed on *Hb. mobilis*.[15] The strong contribution from the DR mechanism indicates that the cofactor arrangement in Braunstoff may be similar to the pigment orientation in R26 RCs.

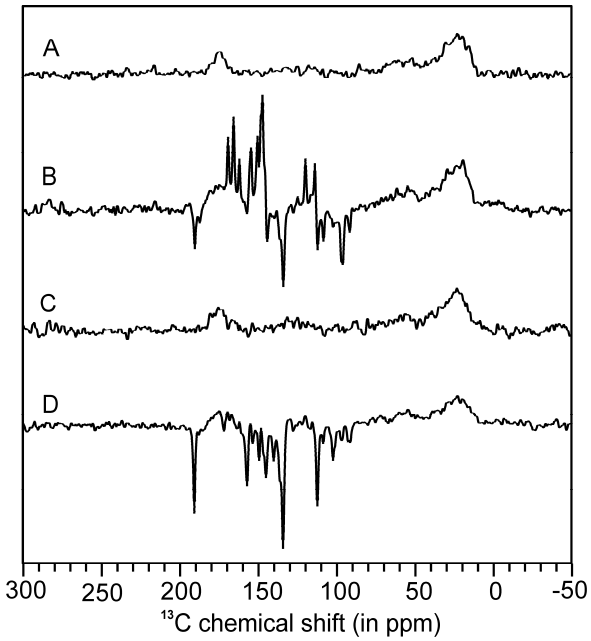

Figure 2.6:^{13}C MAS NMR spectra of anaerobically (Braunstoff) and aerobically (Grünstoff) treated cells of *Hb. mobilis* obtained by illumination with continuous white light (B and D) and the data collected in the dark (A and C).

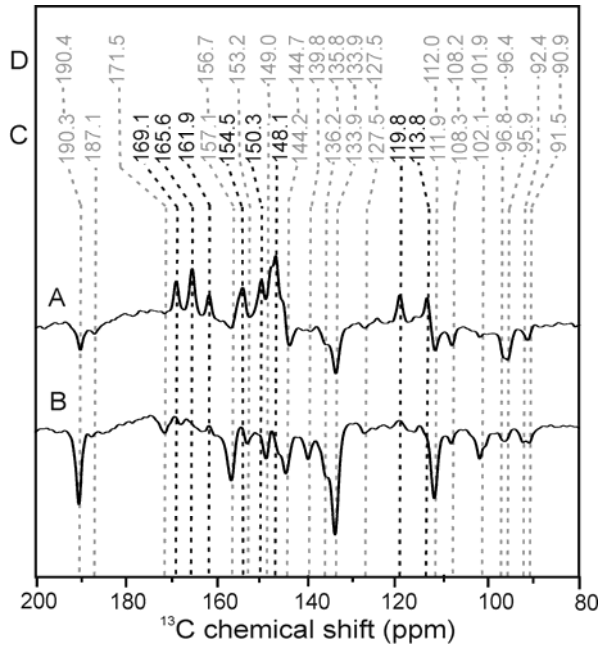

Figure 2.7: Aromatic part of the ^{13}C photo-CIDNP MAS NMR spectra of anaerobically (Braunstoff) (A) and aerobically (Grünstoff) (B) treated cells of *Hb. mobilis*. Lower row of chemical shifts C belong to Braunstoff and the assignments in the upper row D belong to Grünstoff. Black dashed lines point to the absorptive peaks and gray dashed lines indicate emissive peaks.

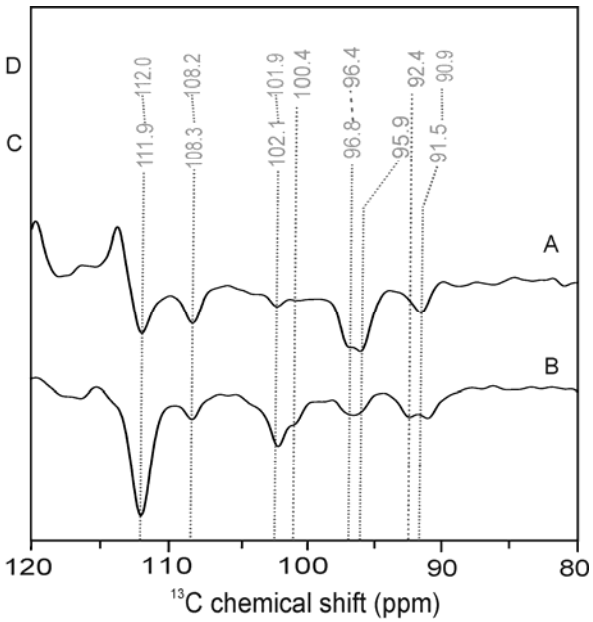

Figure 2.8: The methine region of ^{13}C photo-CIDNP MAS NMR spectra of anaerobically (Braunstoff) (A) and aerobically (Grünstoff) (B) treated cells of *Hb. mobilis*. Chemical shifts in the lower row C belong to Braunstoff and the assignments in the upper row D belong to Grünstoff.

The emissive signals cannot be explained by the DR mechanism.[19] These are attributed to a contribution from the TSM mechanism that is strong relative to the DD mechanism and involves the acceptor. Upon conversion, all the photo-CIDNP signals contribute to the emissive pattern that marks the TSM mechanism, even though the chemical shifts of the signals are almost the same as for the signals in Braunstoff (Figure 2.7).

Figure 2.7 shows an expanded view of the aromatic region of the ^{13}C photo-CIDNP MAS NMR spectra of n.a. Braunstoff and Grünstoff cells. The chemical shifts from Braunstoff (lower row of values C) and Grünstoff (upper row of values D) are compared with the chemical shifts of Chl *a* and BChl *a* obtained from other photo-CIDNP studies in Table 2.2. Apparently the interaction between the cofactors is modified, leading to different activities of the three competing mechanisms. In Grünstoff, the emissive character of the signals can be explained by decay through the singlet channel with T_s = 20 ns, which leads to an enhanced contribution of TSM mechanism[23] over the DR mechanism, for instance due to a change in electron-electron coupling. The negative signal at 190.3 ppm can be

Carbon No.	Chl *a* [a]	BChl *a* [b]	*Hb. mobilis* (Braunstoff)[c]	*Hb. mobilis* (Grünstoff)[c]
13^1	190.6	188.2	190.3(E)^2	190.1(E)^2
17^3	175.3	174.0		
13^3	171.2	171.4		
19	170.2	168.9	165.6(A)^1	165.6(A)^1
14	162.0	160.7	161.1(A)^3	
1	155.9	153.5	154.5(A)^1	154.5(A)^1, 156.7(E)^1
6	154.4	170.2	169.1(A)^1	169.1(A)^1 171.5(E)^1
16	154.0	150.1	150.3(A)^3	153.2(E)^3
4	150.7	152.2	148.1(A)^3	153.2(E)^3
11	147.2	147.2	145.8(A)^1	145.8(A)^1
9	147.2	158.0	150.2(A)^3	149.0(E)^3
8	146.2			144.7(E)^1
8^1			64.3(E)^2	64.3(E)^2
3	137.0	136.1		139.8(E)^1
2	136.1	140.1	133.9(E)^2	133.9(E)^2
12	134.0	119.9	119.8(A)^2	119.8(A)^2
7	133.4		43.5(A)^2	43.5(A)^2
13	126.2	124.1	127.5(E)^1	127.5(E)^1
3^1	126.2	194.5	113.8(A)^2	113.8(A)^2
3^2	113.4		111.9(E)^3	112.0(E)^3
10	108.2	100	108.3(E)^3	108.2(E)^3
15	102.8	105.8	102.1(E)^3	101.9(E)^3, 100.4(E)^3
5	98.1	98.8	96.8(E)^3,95.9(E)^3	96.4(E)^3
20	93.3	93.7	91.5(E)^3	92.4(E)^3, 90.9(E)^3
17	51.4		52.4(A)^1	52.4(A)^1
17^1			29.0(A)^2	
18			47.1(A)^2	

Table 2.2: Preliminary assignments of ^{13}C photo-CIDNP MAS NMR signals in the spectra of Braunstoff and Grünstoff. Labels (A) indicate absorptive and (E) emissive signals, respectively. [a] Ref. 43; [b]Ref 32; [c] this work: The superscripts 1,2,3 in the chemical shifts corresponds to the assignments from 4-ala, 3-ala and unlabelled heliobacterial cells respectively

assigned to the C-13^1 carbonyl carbon atom of the acceptor 8^1-OH Chl a_F. The positive signals at 169.1, 165.6, 161.9, 154.5 150.3, 148.1, 119.8 and 113.8 ppm, which are absent in the spectra of Grünstoff, can be tentatively assigned to carbon atoms C-6, C-19, C-14, C-1, C-16, C-4, C-12 and C-3^1, respectively, of the donor BChl *g*. The negative signals at 171.5, 157.1, 153.2, 149.0, 144.7, 139.8, 133.9 and 112 ppm match well to C-6, C-1, C-16, C-9, C-8, C-3, and C-3^2 carbon atoms of

acceptor 8^1-OH Chl a_F. These assignments of BChl g' and 8^1-OH Chl a_F are based on the comparison with the data obtained for Chl *a* and Bchl *a* in the RCs of PSI and *Rb. sphaeroides* (see Table 2.2). Hence, the chemical shift patterns show that in Braunstoff all the light induced absorptive signals are due to BChl g' (the electron donor) and in both forms the emissive signals are due to 8^1-OH Chl a_F (the electron acceptor).

The signals in the methine region show an emissive pattern in both Braunstoff and Grünstoff (for an expanded view, see Figure 2.8). The signals at 108.3 and 102.1 ppm are attributed to ^{13}C-10 and ^{13}C-15 carbon nuclei of 8^1-OH Chl a_F, respectively. The methine carbon atom C-5 is observed as a doublet (96.8 and 95.9 ppm) in Braunstoff, while in Grünstoff only a single signal (96.4 ppm) occurs. On the other hand, the methine carbon atom C-20 in Grünstoff is split (92.4 and 90.9 ppm) but not in Braunstoff (91.5 ppm). Since in both cases the negative signals originate from the acceptor, we conclude from the splitting that in both forms the two acceptor branches are active, and that the acceptors are slightly distinguishable and are probably the two acceptor 8^1-OH Chl a_F molecules. The activity of both branches of cofactors, as measured by the photo-CIDNP signal intensity pattern, is similar to that found for PSI.[44]

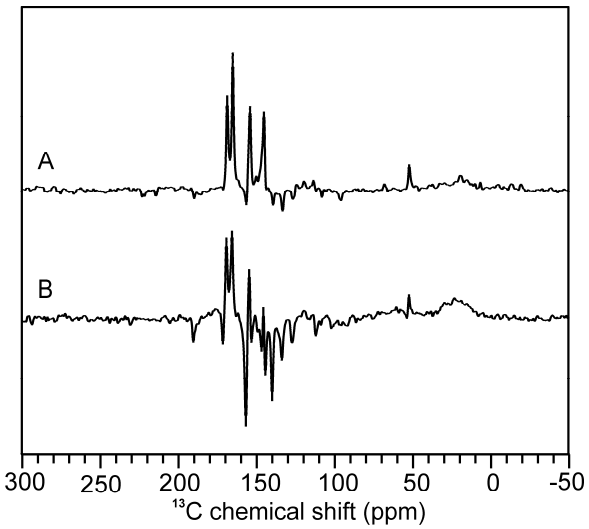

Figure 2.9: ^{13}C photo-CIDNP spectra of 4-ALA *Hb. mobilis* cells, anaerobically (Braunstoff) (A) and aerobically (Grünstoff) (B) treated. The spectra have been obtained by illumination with continuous white light in a magnetic field of 4.7 T and at a temperature of 235 K.

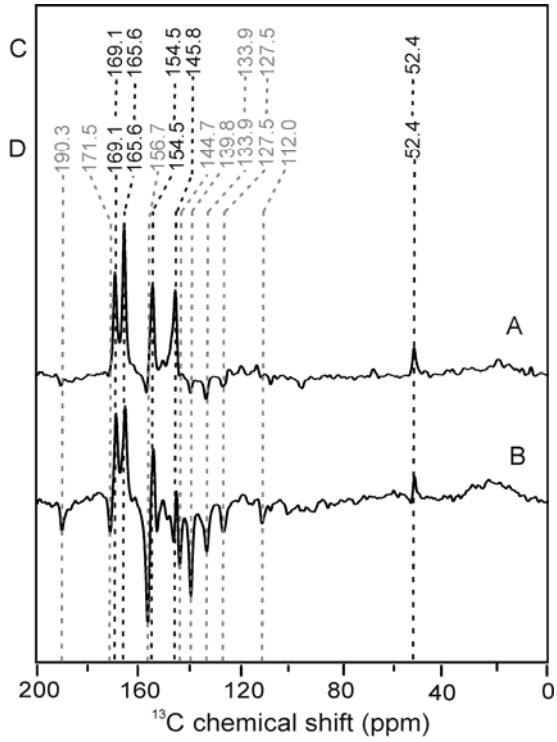

Figure 2.10: Expanded view of the ^{13}C photo-CIDNP MAS NMR spectra of anaerobically (Braunstoff) (A) and aerobically (Grünstoff) (B) treated cells of 4-ALA labelled *Hb. mobilis*. Chemical shifts in the upper row C belong to Braunstoff and the assignments in the lower row D belong to Grünstoff. Black dashed lines indicate the absorptive peaks and gray dashed lines correspond with emissive peaks.

2.4.3 *^{13}C photo-CIDNP MAS NMR on selectively ^{13}C labeled samples.*

Selective enhancement of ^{13}C photo-CIDNP MAS NMR signals by isotope labeling can help in the assignment of the light-induced signals. ^{13}C isotope labeling of the cofactors has been achieved in the RCs of Braunstoff and Grünstoff by biosynthetic incorporation of labels, using selectively labeled ALA as precursor (Figure 2.2). The position of the ^{13}C label in the RC cofactors depends on the position of the ^{13}C label in the precursor ALA. Both 4-^{13}C ALA and 3-^{13}C ALA precursors have been used in this study.

^{13}C photo-CIDNP MAS NMR spectra of 4-^{13}C ALA labeled *Hb. mobilis* cells are shown in Figure 2.9. Spectra A and B originate from Braunstoff and Grünstoff, respectively. Apart from the signals in the aromatic region, one light induced signal is observed in the aliphatic region in both spectra. It originates from C-17 of the donor, which gains signal intensity via ^{13}C-^{13}C spin diffusion from the

nearby aromatic carbons of the cofactor.[22] In the spectrum of Braunstoff, only absorptive signals are strongly enhanced. In the spectrum of Grünstoff, both strongly enhanced positive and negative signals are observed. A shift of intensity from negative to positive signals upon isotope labeling is evident and demonstrates that magnetic nuclei actively participate in the spin dynamics. Interestingly, for the 3-ALA labeled sample (Figure 2.11), in which the magnetic isotopes are more distant from the π-system, the shift of intensity is less pronounced. Since isotope labeling modifies the photo-CIDNP intensities, the concentration of isotope label is difficult to extract by comparing signals from labeled and unlabeled positions. However, in 2-dimensional experiments cross-peaks were difficult to detect (data not shown), which indicates a label incorporation below 50%.

The expanded view of the light induced signals from 4-^{13}C ALA labeled *Hb. mobilis* cells in both forms is presented in Figure 2.10. The absorptive light-induced signals with chemical shifts of 165.6, 154.5, 169.1 and 145.8 ppm can be attributed to to C-19, C-1, C-6, and C-11 of the donor BChl *g'* (see black labels in the Figure 2.2 A) in both Braunstoff and Grünstoff (see Table 2.2). The absorptive signal in the aliphatic region at 52.4 ppm belongs to C-17 of BChl *g'* which is the only aliphatic carbon that is ^{13}C labeled when using a 4-^{13}C ALA

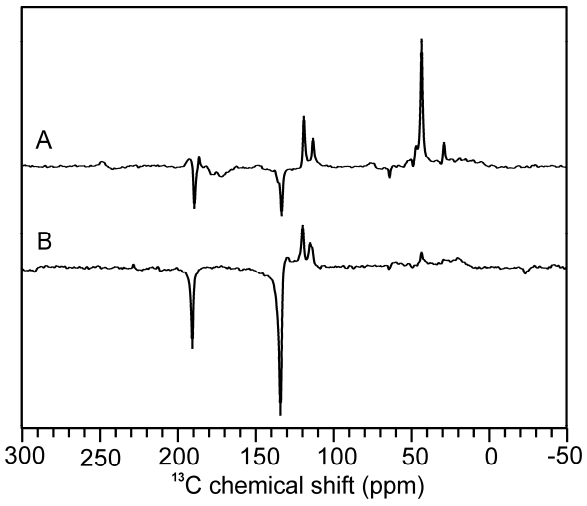

Figure 2.11: ^{13}C photo-CIDNP spectra of 3-ALA *Hb. mobilis* cells, anaerobically (Braunstoff) (A) and aerobically (Grünstoff) (B) treated. The spectra have been obtained by illumination with continuous white light in a magnetic field of 4.7 T and at a temperature of 235 K.

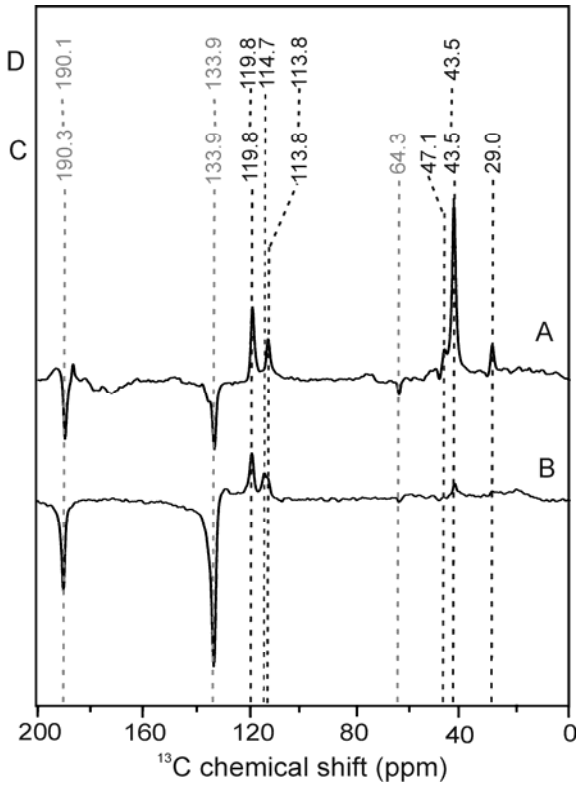

Figure 2.12: Expanded view of the ^{13}C photo-CIDNP MAS NMR spectra of anaerobically (Braunstoff) (A) and aerobically (Grünstoff) (B) treated cells of 3-ALA labeled *Hb. mobilis*. Chemical shifts in the lower row belong to Braunstoff and the assignments in the upper row belong to Grünstoff. Black dashed lines indicate the absorptive peaks and gray dashed lines correspond with emissive signals.

labeled substrate. The emissive light induced signals with chemical shifts of 156.7. 171.5, 144.7, 139.8, and 127.5 ppm can be attributed to the C-1, C-6, C-8, C-3, and C-13 of the primary acceptor 8^1-OH Chl a_F (see black labels in Figure 2.2 B and Table 2.2). Again, it is evident that the donor and acceptor cofactors both give rise to a unique NMR response. Since the chemical shift pattern remains the same in the conversion from Braunstoff to Grünstoff, the functional symmetry and identity of the active cofactors appears not affected by the transition

In the ^{13}C photo-CIDNP MAS NMR spectra of 3-^{13}C ALA labeled *Hb. mobilis* cells (Figure 2.11 and Figure 2.12), the spectrum of Braunstoff (A) shows mixed patterns of absorptive and emissive light induced signals. That the signal intensity of the positive signal in the aliphatic region (43.5 ppm, C-7 of the donor)

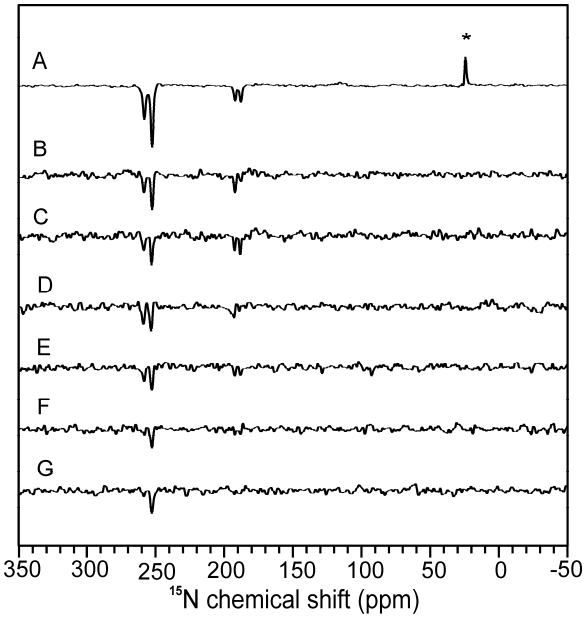

Figure 2.13: Series of time-resolved ^{15}N photo-CIDNP spectra of uniformly ^{15}N labeled *Hb. mobilis* cells, anaerobically treated (Braunstoff). The spectra have been obtained in a magnetic field of 4.7 T and at a temperature of 235 K. The laser pulses have a length of ~10 ns and a wavelength of 532 nm. The delay times between the laser pulse and the start of NMR data acquisition is 0 µs (B), 10 µs (C), 30 µs (D), 50 µs (E), 100 µs (F), 200 µs (G). The spectrum at the top (A), obtained with continuous illumination, is shown for comparison.

is stronger than for labeled aromatic carbons might be due to local dynamics.[45] The positive signals in the aliphatic region are due to carbons C-7, C-17^1 and C-18 of the primary donor BChl *g*' (see gray labels in Figure 2.2 A and Table 2.2). The resolved response at 29.0 ppm originates from C-17^1 of the donor, while the only emissive signal in the aliphatic region occurs at 64.3 ppm and can be tentatively assigned to C-8^1 of the acceptor. The weak negative signals near to the 29 and 47 ppm signals belong to C-17^1 and C-18 of the primary acceptor 8^1-OH Chl a_F (see gray labels in Figure 2.2 B and Table 2.2). Hence, the isotope labeling experiment supports the assignment of the positive signals to the donor cofactor and of the negative signals to the acceptor cofactor.

The absorptive signals at 119.8 and 113.8 ppm in the aromatic region correspond to the C-12 and C-13 carbon atoms of BChl *g*' (Table 2.2). The emissive light-induced signals at 190.3 and 133.9 ppm correspond with the C-13^1 and C-2 carbon atoms of the acceptor 8^1-OH Chl a_F (Table 2.2). These are the most

intense signals in the spectrum of Grünstoff. Table 2.2 summarizes the assignments. There is one absorptive signal originating from the C-3^1 carbon atom of the BChl *g*' donor in the spectrum of Grünstoff that appears to be doubled (113.8 and 114.7 ppm). In both spectra, positive and negative signals appear to be very narrow, with almost equal linewidths of ~35 Hz. The observation of very sharp lines from the cofactors seems to be a general feature of RCs,[34,38,42] providing a well defined, homogeneously ordered, dynamically averaged, environment. These features remain intact upon photoconversion to Grünstoff.

2.4.4 *Time-resolved -photo-CIDNP MAS NMR experiments*

Time-resolved photo-CIDNP MAS NMR experiments allow for observation of the evolution of spin dynamics and of the reaction kinetics of the radical pair on a microsecond timescale.[22,32] Here we report time-resolved data obtained from both Braunstoff and Grünstoff by solid-state photo-CIDNP MAS NMR experiments on ^{15}N uniformly labeled as well as on 3-^{13}C ALA labeled *Hb. mobilis* cells using nanosecond laser flashes. The time resolution was obtained by varying the delay time Δ, which is the time difference between the laser pulse and the beginning of the NMR $\pi/2$ detection pulse (see Figure 2.3).

Figure 2.13 shows the photo-CIDNP ^{15}N MAS NMR spectra of *Hb. mobilis* cells (Braunstoff). The top spectrum (A) is the photo-CIDNP MAS NMR response obtained with continuous illumination of white light. The other traces represent the time-resolved photo-CIDNP MAS NMR data obtained by varying the delay time from Δ = 0 μs (B) to Δ = 200 μs (G). In the spectrum with Δ=0 μs (B), four signals with chemical shifts of 188.4, 258.8, 193.1, 253.0 ppm occur, attributed to the N-I, N-II, N-III, N-IV nitrogen atoms of BChl *g*', respectively. The spectra were collected with a delay time Δ of 10 (C), 30 (D), 50 (E), 100 (F) or 200 μs (G). Compared with the spectrum obtained with continuous illumination, these time-resolved spectra show a lower signal to noise ratio. The intensity of light induced signals decays with an increase in the delay time from 0 μs to 100 μs, especially for the signals at chemical shifts of 188.4 (attributed to N-I) and 193.1 (attributed to N-III) ppm. The light-induced signal at 253 ppm persists at a delay time of 200 μs and

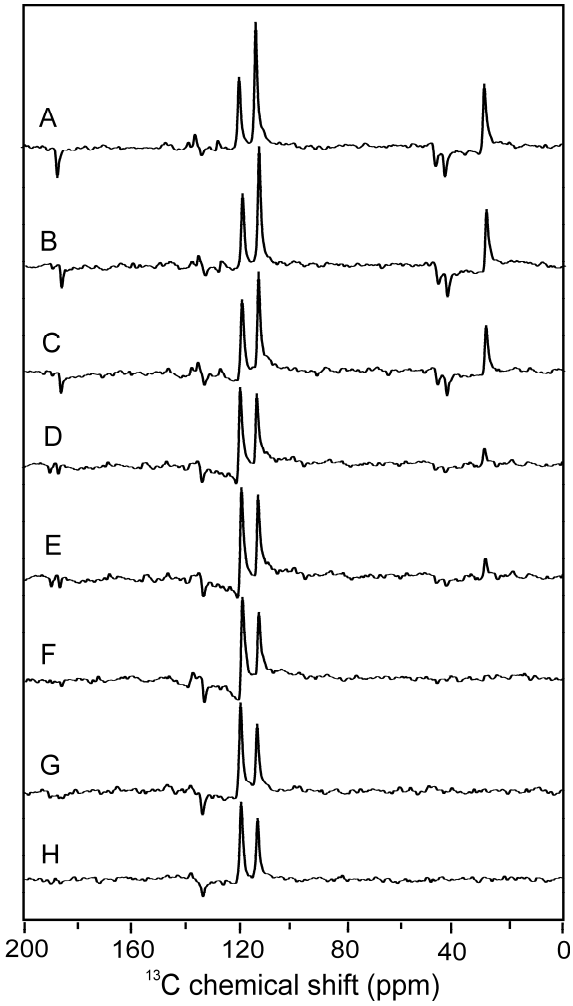

Figure 2.14: Series of time-resolved ^{13}C photo-CIDNP MAS NMR spectra of 3-ALA labeled *Hb. mobilis* cells, anaerobically (Braunstoff) treated. The spectra have been obtained in a magnetic field of 4.7 T and at a temperature of 235 K. The laser pulses have a length of ~10 ns and a wavelength of 532 nm. The delay time between laser pulse and NMR measurement is 0 μs (A), 10 μs (B), 30 μs (C), 50 μs (D), 100 μs (E), 200 μs (F), 500 μs (G) and 1 ms (H).

longer. As shown in Scheme 2.1, the transient signals are due to the RPM polarization of the cofactors that are in the ground state following the rapid decay via the singlet channel with T_s = 20 ns, and are observable until the nuclear spin population of the cofactors that reach the ground state from the triplet leads to the recovery of the Boltzmann equilibrium and quenching of the light-induced enhancement on the time scale of the donor triplet lifetime τ =~100 μs. A very similar pattern of decay of light induced signals with increase of delay time and life time (τ) of donor triplet was observed in time-resolved photo-CIDNP MAS NMR

measurements of *Rb. sphaeroides* R26.[39] In the time evolution of Braunstoff, the same kinetics, at a time scale τ =~100 μs, is found in the parallel decay of three signals, while steady state nuclear polarization builds up leading to the dominant signal at 253.0 ppm. This would imply that, similar to *Rb. spheroides* R26, Braunstoff has a long-lived ^{3}P state which is not quenched by nearby carotenoids.

From 3-^{13}C ALA labeled *Hb. mobilis* cells, high-quality time-resolved photo-CIDNP spectra have been obtained. A set of laserflash photo-CIDNP spectra of Braunstoff with different delay time Δ is shown in Figure 2.14. The data collected with a delay time of 0 μs (A) show the light-induced signals almost similar to the steady state photo-CIDNP MAS NMR spectra of 3-^{13}C ALA labeled Braunstoff (see Figure 2.11A), except for the absence of the emissive signal at 133.9 ppm, the occurrence of the signal at 187.0 ppm and for the different phasing of the signals in aliphatic region. The signals in the aliphatic region disappear within about 100 μs, confirming the transient nuclear polarization from cofactors in their ground state in the time window 20ns <Δ<100 μs, *i.e.* between the rapid decay from the singlet state and the slower decay from the triplet state.[22] In the same time interval, also the transient signal of the carbonyl carbon at 187.0 ppm disappears and the emissive signal at 133.9 ppm evolves. After 100 μs, the light-induced signals are due to the steady state photo-CIDNP effect. Hence, the time evolution clearly demonstrates (i) the occurrence of a long-lived ^{3}P donor triplet state in Braunstoff by the observation of transient nuclear polarization associated with the rapidly decaying singlet component of the radical pair that (ii) confirms a triplet lifetime τ = ~100 μs (Scheme 2.1), which (iii) matches the kinetics reported for *Rb. sphaeroides* R26.[22]

Figure 2.15 shows a series of time resolved photo-CIDNP ^{13}C MAS NMR datasets collected from 3-^{13}C ALA labeled cells of Grünstoff. This transient nuclear polarization is similar to that observed in Braunstoff since the transient features disappear on a timescale of 100 μs. The similarity of the spectral features of the transient nuclear polarization as well as the conservation of its decay kinetics, demonstrate that the identity of the cofactors forming the radical pair is not changed upon phototransformation. There is, however, a remarkable difference in the time-evolution of both forms. Unlike the time resolved spectrum of Braunstoff,

light-induced signals are observed in the time resolved spectrum of Grünstoff after the initial 10 μs (Figure 2.15). Such a 'silent' initial period has not yet been reported from other RCs. Except for the signal at 133.9 ppm, the signals decay for $\Delta > 100$ μs (data not shown). This demonstrates that Grünstoff has a triplet lifetime $\tau = 100$ μs, similar to the Braunstoff, and for $\Delta<100$ μs the polarization from the RC fraction subject to recombination via the singlet channel is observed (Scheme 2.1).

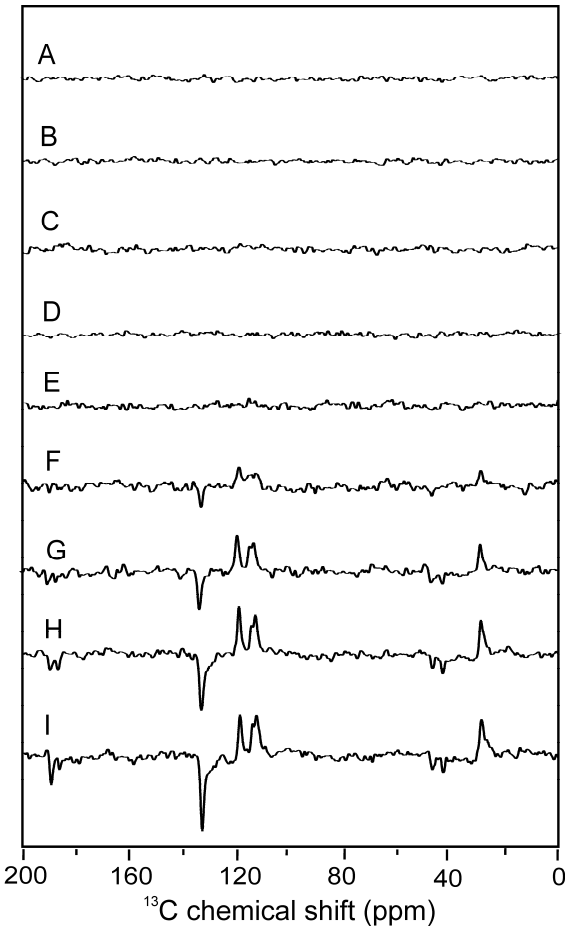

Figure 2.15: Series of time-resolved ^{13}C photo-CIDNP MAS NMR spectra of 3-ala labelled *Hb. mobilis* cells, aerobically (Grünstoff) treated. The spectra have been obtained in a magnetic field of 4.7 T and a temperature of 235 K. The laser pulses have a length of ~10 ns and a wavelength of 532 nm. The delay time between laser pulse and NMR measurement is 0 μs (A), 3 μs (B), 5 μs (C), 7 μs (D), 8 μs (E), 9 μs (F), 10 μs (G), 30 μs (H) and 50 μs (I).

2.5 *Discussion*

2.5.1 *Structure of the primary radical pair in Braunstoff*

The solid state photo-CIDNP data provide converging evidence that the overall radical pair structure and kinetics in *Hb. mobilis* are similar to those in RCs of *Rb. sphaeroides* R26. The positive sign of the donor signals, the proposed occurrence of the DR mechanism[15] and in particular the triplet lifetime τ = 100 μs match very well with the data from R26 RCs. It is tempting to conclude that *Hb. mobilis* has a similar cofactor arrangement as for the R26 RCs, with a central special pair, accessory cofactors and primary acceptor cofactors leading to a similar dynamics of electron transfer and triplet lifetime in the two species. The triplet kinetics obtained from time resolved experiments provides evidence for a long lived donor triplet state that is not quenched by carotenoids, similar to the case of R26 RCs.

In such a scheme, any difference with the heterodimeric R26 RCs would be due to the homodimeric symmetry of the subunits in heliobacterial RCs. Alternatively, dynamic symmetry breaking of the homodimer may lead to a monomeric (accessory) chlorophyll carrying the donor charge and not a dimeric primary donor, similar to PSII.[46] The heterodimeric nature of R26 RCs leads to different chemical shifts for the two donor cofactors in the photo-CIDNP MAS NMR spectra of R26 RCs.[21] In *Hb mobilis* there is no indication for signal doubling at the donor site. At the acceptor site, a clear doubling occurs in the methine carbon region, since five instead of four signals are present. The resonances with shifts of 96.8 and 95.9 ppm and with the same intensity (Figure 2.8), are assigned to the C-5 of 8^1-OH Chl a_F cofactors. Hence, at the acceptor side a very minor difference occurs, which can be reconciled with minor symmetry breaking of the homodimer, if both branches are equally active. A similar functional symmetry of acceptor cofactors is found in PSI.[44]

2.5.2 *Structure of the early radical pair in Grünstoff*

The chemical shift patterns for the absorptive and emissive signals in Braunstoff and Grünstoff are virtually identical, and this confirms the identity of the chemical structure of the radical pair in both forms. Also for Grünstoff both

branches appear to be active, as shown by the slight doubling of the signals at 92.4/90.6 (C-20) and 101.9/100.4 (C-15) (Figure 2.8). There might be a slight asymmetry of intensities observable at the C-5 signal of the acceptor at about 96.4 ppm. That the functional symmetry remains upon phototransformation demonstrates that the general radical pair structure remains unchanged and is robust. In particular, the phototransformation acts symmetrically on both parts of the homodimer.

There are two significant differences between the spectra of Braunstoff and Grünstoff: (i) The ratio between absorptive and emissive signals is shifted. This is certainly due to a weakening of the effect of DR in the first 10 μs, as demonstrated in the time-resolved experiments. It might indicate a difference in the composition of the contributions of the solid-state photo-CIDNP mechanisms in favour of the TSM, which contributes to the inversion of signals in Grünstoff. (ii) The occurrence of the 'silent' initial phase in the triplet evolution of Grünstoff while signals are visible in the case of Braunstoff. While after 10 μs the donor triplet state is localized and produces signal enhancement, it appears that the localization is preceded by early mobility of either the radical cation or the donor triplet state. This can be explained by the change of environment near the donor cofactor due to the involvement of accessory cofactors in early charge separation. Since the radical cation decays on the ns timescale, the observed dynamics is due to the donor triplet. In fact, complex dynamics in the excited state with coexistence of different charge transfer channels and mobility of the donor triplet state has been resolved for PS II, with the radical cation state and the ^{3}P680 located on a monomeric (accessory) chlorophyll and not on the dimeric primary donor.[47,46] Also for *Hb. mobilis*, the excitation dynamics appears complex with possibly a mobile donor triplet formed on another cofactor, most likely a photoconverted accessory cofactor, before it settles after 10 μs and forms the radical pair state that is active in the photo-CIDNP.

2.5.3 *Functional flexibility*

The accessory cofactor appears to be modified by the phototransformation from BChl *g* to Chl a_F. The presence of a donor triplet state on accessory chlorophylls has been reported in PSII at cryogenic temperature.[48,49] Most likely

Grünstoff carries the donor triplet on a accessory cofactor which resembles PSII rather than PSI. In both plant RCs an accessory pigment also acts as the primary electron donor,[50-53] although on an NMR timescale the stabilized radical pair is observed.[38,54] Similarly, charge separation in RCs of *Rb. sphaeroides* that occurs with the participation of accessory pigments is observed on the time-scale of an NMR experiment as a radical cation of the special pair.[55] Here, the radical pair observed in the Grünstoff might not be the primary radical pair, but a product of a stabilization process on the sub-μs timescale.

The RCs of heliobacteria have been proposed to be ancestors of PSI. On the one hand, bidirectional electron transfer is a feature of PSI. On the other hand, the possible involvement of an accessory cofactor in triplet formation is reminiscent of PSII, although heliobacterial RCs do not appear to be an evolutionary ancestor of PSII. This would imply that the function of RCs is rather flexible. RCs maintain a general cofactor architecture, which can be homodimeric or not, which is functionally robust for changes of the matrix, which simply lead to changes of the pathways but not a change of function. The transformation of heliobacteria confirms the remarkable combination of robustness, efficiency and flexibility of natural RCs.

The root of the photosynthesis phylogenetic tree has been difficult to ascertain. Assuming that all photosynthetic RCs have been evolved from a common homodimeric ancestor,[56,57] heliobacteria might be placed near to this ancestor, very early in evolution.[58] The remarkable flexibility of heliobacterial RCs, as demonstrated here, might have allowed for branching into type-I and type-II RCs, in an evolutionary scheme where optimization of photosynthesis for energy conversion and use as a primary biological selection criterion.

References

(1) Gest, H. *Photosyn. Res*. **1994**, 41, 17-21.

(2) Stevenson, A. K.; Kimble, L. K.; Woese, C. R.; Madigan, M. T. *Photosyn. Res.* **1997**, *53*, 1-11.

(3) Golbeck, J. *Photosyn. Res.* **2007**, *91*, 139-140.

(4) Vassiliev, I. R.; Antonkine, M. L.; Golbeck, J. H. *Biochim. Biophys. Acta.* **2001**, *1507*, 139-60.

(5) Nitschke, W.; Rutherford, A. W. *Trends. Biochem. Sci.* **1991**, *16*, 241-5.

(6) Liebl, U.; Mockensturmwilson, M.; Trost, J. T.; Brune, D. C.; Blankenship, R. E.; Vermaas, W. *Pro. Natl. Acad. Sci. USA* **1993**, *90*, 7124-7128.

(7) Olson, J. M.; Blankenship, R. E. *Photosyn. Res.* **2004**, *80*, 373-386.

(8) Gest, H.; Favinger, J. L. *Arch. Microbiol.* **1983**, *136*, 11-16.

(9) Brockmann, H.; Lipinski, A. *Arch. Microbiol.* **1983**, *136*, 17-19.

(10) Kobayashi, M.; Vandemeent, E. J.; Erkelens, C.; Amesz, J.; Ikegami, I.; Watanabe, T. *Biochim. Biophys. Acta* **1991**, *1057*, 89-96.

(11) van de Meent, E. J.; Kobayashi, M.; Erkelens, C.; Vanveelen, P. A.; Amesz, J.; Watanabe, T. *Biochim. Biophys. Acta* **1991**, *1058*, 356-362.

(12) Amesz, J. *J. Photochem. Photobio.* **1995**, *30*, 89-96.

(13) Nabedryk, E.; Leibl, W.; Breton, J. *Photosyn. Res.* **1996**, *48*, 301-308.

(14) Prince, R. C.; Gest, H.; Blankenship, R. E. *Biochim. Biophys. Acta* **1985**, *810*, 377-384.

(15) Roy, E.; Rohmer, T.; Gast, P.; Jeschke, G.; Alia, A.; Matysik, J. *Biochemistry* **2008**, *47*, 4629-4635.

(16) Zysmilich, M. G.; McDermott, A. *J. Am. Chem. Soc.* **1994**, *116*, 8362-8363.

(17) Matysik, J.; Diller, A.; Roy, E.; Alia, A. *Photosyn. Res.* **2009**, *102*, 427-435.

(18) Daviso, E.; Jeschke, G.; Matysik, J. in Biophysical Techniques in Photosynthesis II (Aartsma T.J., Matysik, J., eds.), Springer Dordrecht, pp. 385-399 (**2008**).

(19) Jeschke, G.; Matysik, J. *Chem. Phy.s* **2003**, *294*, 239-255.

(20) Prakash, S.; Alia; Gast, P.; de Groot, H. J. M.; Jeschke, G.; Matysik, J. *J. Am. Chem. Soc.* **2005**, *127*, 14290-14298.

(21) Prakash, S.; Alia; Gast, P.; de Groot, H. J. M.; Matysik, J.; Jeschke, G. *J. Am. Chem. Soc.* **2006**, *128*, 12794-12799.

(22) Daviso, E.; Alia, A.; Prakash, S.; Diller, A.; Gast, P.; Lugtenburg, J.; Matysik, J.; Jeschke, G. *J. Phys. Chem. C* **2009**, *113*, 10269-10278.

(23) Jeschke, G. *J. Chem. Phys.* **1997**, *106*, 10072-10086.

(24) Polenova, T.; McDermott, A. E. *J. Phys. Chem. B* **1999**, *103*, 535-548.

(25) McDermott, A.; Zysmilich, M. G.; Polenova, T. *Solid State Nucl. Mag. Res.* **1998**, *11*, 21-47.

(26) Goldstein, R. A.; Boxer, S. G. *Biophys*. *J*. **1987**, *51*, 937-946.

(27) Closs, G. L. *Chem*. *Phys*. *Lett*. **1975**, *32*, 277-278.

(28) Janssen, G. J.; Daviso, E.; van Son, M.; de Groot, H. J. M.; Alia, A.; Matysik, J. *Photosyn. Res.* **2010**, *104*, 275-282.

(29) Daviso, E.; Janssen, G. J.; Alia, A.; Jeschke, G.; Matysik, J.; Tessari, M. *J. Am. Chem. Soc.* **2011**, *133*, 16754-16757.

(30) Jeschke, G.; Anger, B. C.; Bode, B. E.; Matysik, J. *J. Phys. Chem. A* **2011**, *115*, 9919-9928.

(31) Daviso, E.; Diller, A.; Alia, A.; Matysik, J.; Jeschke, G. *J. Magn. Reson.* **2008**, *190*, 43-51.

(32) Van de Meent, E. J.; Kleinherenbrink, F. A. M.; Amesz, J. *Biochim. Biophys. Acta* **1990**, *1015*, 223-230.

(33) Schulten, E. A. M.; Matysik, J.; Alia; Kiihne, S.; Raap, J.; Lugtenburg, J.; Gast, P.; Hoff, A. J.; de Groot, H. J. M. *Biochemistry* **2002**, *41*, 8708-8717.

(34) Fischer, M. R.; de Groot, H. J. M.; Raap, J.; Winkel, C.; Hoff, A. J.; Lugtenburg, J. *Biochemistry* **1992**, *31*, 11038-11049.

(35) Matysik, J.; Alia; Hollander, J. G.; Egorova-Zachernyuk, T.; Gast, P.; de Groot, H. J. M. *Indian J. Biochem. Biophys.* **2000**, *37*, 418-423.

(36) Matysik, J.; Schulten, E.; Alia; Gast, P.; Raap, J.; Lugtenburg, J.; Hoff, A. J.; de Groot, H. J. M. *Biol. Chem.* **2001**, *382*, 1271-1276.

(37) Bennett, A. E.; Rienstra, C. M.; Auger, M.; Lakshmi, K. V.; Griffin, R. G. *J. Chem. Phys.* **1995**, *103*, 6951-6958.

(38) Diller, A.; Roy, E.; Gast, P.; van Gorkom, H. J.; de Groot, H. J. M.; Glaubitz, C.; Jeschke, G.; Matysik, J.; Alia, A. *Pro. Natl. Acad. Sci. USA* **2007**, *104*, 12767-12771.

(39) Daviso, E.; Prakash, S.; Alia, A.; Gast, P.; Jeschke, G.; Matysik, J. *Appl. Magn. Reson.* **2010**, *37*, 49-63.

(40) Prakash, S.; Tong, S. H.; Alia, A.; Gast, P.; Jeschke, G.; Matysik, J. in Photosynthesis: Fundamental Aspect to Global Perpectives, (A. ed. by van der Est, A. Bruce), Allen Press Montreal, pp. 236-237, (**2005**).

(41) Eisenmayer, T. J.; de Groot, H. J. M.; van de Wetering, E.; Neugebauer, J.; Buda, F. *J. Phys. Chem. Lett.* **2012**, *3*, 694-697..

(42) Matysik, J.; Alia; Gast, P.; van Gorkom, H. J.; Hoff, A. J.; de Groot, H. J. M. *Pro. Natl. Acad. Sci. USA* **2000**, *97*, 9865-9870.

(43) Boender, G. J . (1996) Ph.D. Thesis, University of Leiden, Leiden, The Netherlands.

(44) Santabarbara, S.; Kuprov, I.; Fairclough, W. V.; Purton, S.; Hore, P. J.; Heathcote, P.; Evans, M. C. W. *Biochemistry* **2005**, *44*, 2119-2128.

(45) Sai Sankar Gupta, K. B. (2011) Ph.D. Thesis, University of Leiden, Leiden, The Netherlands.

(46) Novoderezhkin, V. I.; Romero, E.; Dekker, J. P.; Van Grondelle, R. *Chem. Phys. Chem.* **2011**, *12*, 681–688.

(47) Lubitz, W.; Lendzian, F.; Bittl, R. *Acc. Chem. Res.* **2002**, *35*, 313-320

(48) Lendzian, F.; Bittl, R.; Telfer, A.; Lubitz, W. *Biochim. Biophys. Acta* **2003**, *1605*, 35-46.

(49) Kammel, M.; Kern, J.; Lubitz, W.; Bittl, R. *Biochim. Biophys. Acta* **2003**, *1605*, 47-54.

(50) Muller, M. G.; Niklas, J.; Lubitz, W.; Holzwarth, A. R. *Biophys. J.* **2003**, *85*, 3899-3922.

(51) Holzwarth, A. R.; Muller, M. G.; Niklas, J.; Lubitz, W. *Biophys. J.* **2006**, *90*, 552-565.

(52) Prokhorenko, V. I.; Holzwarth, A. R. *J. Phys. Chem. B* **2000**, *104*, 11563-11578.

(53) Holzwarth, A. R.; Muller, M. G.; Reus, M.; Nowaczyk, M.; Sander, J.; Rogner, M. *Pro. Natl. Acad. Sci. USA* **2006**, *103*, 6895-6900.

(54) Alia; Roy, E.; Gast, P.; van Gorkom, H. J.; de Groot, H. J. M.; Jeschke, G.; Matysik, J. *J. Am. Chem. Soc.* **2004**, *126*, 12819-12826.

(55) van Brederode, M. E.; van Mourik, F.; van Stokkum, I. H. M.; Jones, M. R.; van Grondelle, R. *Pro. Natl. Acad. Sci. USA* **1999**, *96*, 2054-2059.

(56) Xiong, J.; Bauer, C. E.; *Annu. Rev. Plant Bio.* **2002**, *53*, 503-521.

(57) Allen, J. F.; Vermaas, W. F. Evolution of photosynthesis. In: Encyclopedia of Lifesciences (ELS) (2010) John Wiley & Sons, Ltd: Chichster.

(58) Giacometti, G.; Giacometti, G. M.; *Appl. Magn. Reson.* **2010**, *37*, 13-25.